J. Fluid Mech. (2009), *vol.* 634, *pp.* 165–189.
doi:10.1017/S0022112009007149 Printed in the United Kingdom

Mechanisms for spatial steady three-dimensional disturbance growth in a non-parallel and separating boundary layer

OLAF MARXEN[1,2]†, MATTHIAS LANG[1], ULRICH RIST[1], ORI LEVIN[2] AND DAN S. HENNINGSON[2]

[1]Institut für Aerodynamik und Gasdynamik, Universität Stuttgart, Pfaffenwaldring 21, D-70550 Stuttgart, Germany

[2]Linné Flow Centre, KTH Mechanics, SE-100 44 Stockholm, Sweden

(Received 26 November 2007 and in revised form 16 March 2009)

Steady linear three-dimensional disturbances are investigated in a two-dimensional laminar boundary layer. The boundary layer is subject to a streamwise favourable-to-adverse pressure gradient and eventually undergoes separation. The separating flow corresponds to the first part of a pressure-induced laminar-separation bubble on a flat plate. Streamwise disturbance development in such a flow is studied by means of direct numerical simulation, a water-tunnel experiment and an adjoint-based parabolic theory suited to study spatial optimal growth. A complete overview of the disturbance evolution in various areas of the favourable-to-adverse pressure gradient laminar boundary layer is given. Results from all investigation methods show overall good agreement with respect to disturbance growth and shape within the entire domain. In the favourable pressure-gradient region and, again, slightly downstream of separation, transient growth caused by the lift-up effect dominates disturbance behaviour. In the adverse pressure-gradient region, a modal instability is observed. Evidence is presented that this instability is of Görtler type.

1. Introduction

A spatially developing boundary layer usually displaces fluid away from the wall and hence grows downstream. The flow will therefore not be exactly parallel to the wall. This effect decreases downstream but can be intensified or weakened by a sufficiently strong streamwise pressure gradient. A boundary layer subjected to a very strong adverse pressure gradient (APG) will even move away from the wall, resulting in boundary-layer separation. Reattachment of a separated, initially laminar, boundary layer can occur due to viscous diffusion or due to a favourable pressure gradient (FPG). In most cases, however, it is caused by an increase in momentum exchange in wall-normal direction, induced through transition to turbulence. The resulting region from separation S to mean reattachment R is denoted as a laminar-separation bubble (LSB). LSBs appear in several technical applications, such as on laminar profiles of a glider wing at moderate to high angles of attack and on wings of unmanned aerial or remotely piloted vehicles.

† Present address: Center for Turbulence Research, Stanford University, Stanford, CA 94305-3035, USA. Email address for correspondence: olaf.marxen@stanford.edu

Due to a strong instability of the separated shear layer, the transition process in an LSB is often solely governed by a strong amplification of high-frequency essentially two-dimensional or weakly oblique fluctuating disturbances leading to vortex shedding. Nevertheless, the flow usually becomes quickly three-dimensional at transition. Two distinct classes of three-dimensional disturbances can cause such three-dimensionality: steady and high-frequency ones. While the latter class has a frequency of the order of the shedding frequency and has been studied in detail (e.g. Rist 1998, 2002, 2003; Spalart & Strelets 2000), the former has attracted only little attention.

If a strong FPG precedes the APG, steady (or very low-frequency) three-dimensional disturbances are sometimes observed already upstream and early inside the LSB.

Quasi-steady three-dimensional disturbances are also seen for environments with high levels of free-stream disturbance. They occur in applications of laminar-separation control, too, if for instance steady blowing/suction through small holes is applied upstream of the bubble or if vortex generators are present.

This paper is concerned with linear steady three-dimensional disturbance growth in an open, incompressible flow bounded by a wall on one side only. The basic configuration is given by a flat-plate boundary layer subjected to a strong favourable-to-adverse streamwise pressure gradient. The pressure gradient is caused by putting a displacement body into the flow at some distance from the plate. Such a body is small in size and is placed sufficiently far away from the plate so that the flow in the vicinity of the wall keeps its semi-bounded character – in contrast to e.g. a channel flow.

1.1. *Introduction to linear instability and three-dimensional disturbance growth*

An important cause of disturbance growth is a modal instability. We follow the definition of a modal instability given by Bottaro & Luchini (1999, cf. § 3). In short, if we perturb the flow at one location, its response in terms of growth rate and disturbance shape further away from this location does not depend on the details of the excitation. A characteristic of a modal instability is a weak disturbance-shape evolution: the disturbance velocity profile changes downstream only in a similar way as the underlying base-flow velocity profile. Moreover, (typically exponential) growth with the same growth rate can be seen in all velocity components: a distinct preferred state in the sense of the most amplified generic state or eigenstate of the flow exists.

The lift-up effect provides a mechanism for disturbance-energy growth in shear flows with a dominating mean-flow direction. It was discovered in inviscid flows (Ellingsen & Palm 1975; Landahl 1975, 1980). For a stable flow, the corresponding growth rate decreases as the cross-stream velocity diminishes.

1.1.1. *Görtler instability*

Görtler instability (Görtler 1941) is a centrifugal instability, associated with curved streamlines in shear flows. For a boundary layer or shear layer, a concave wall or streamline curvature is required (Saric 1994). Local theory predicts streamwise vortices for a zero pressure gradient (ZPG) boundary layer on a concave surface (Floryan & Saric 1982). The lift-up effect also plays its role in Görtler instability: 'An important feature of steady streamwise vortices within a shear layer is the convection of streamwise momentum in the normal and spanwise directions by very weak ... components of the vorticity. This produces large changes in the mean velocity profiles' (Saric 1994, p. 385).

More recent investigations of Görtler instability take into account non-parallel and non-local effects. They are based on a parabolic set of partial differential equations. Initial conditions are either local eigenfunctions (Lee & Liu 1992) or different generic conditions (Luchini & Bottaro 1998; Bottaro & Luchini 1999). Cossu *et al.* (2000) sought a more general solution by means of an optimization procedure. Bottaro & Luchini (1999) confirmed that for a sufficiently large Görtler number and a sufficient distance downstream, modal disturbance behaviour is found and a normal-mode analysis is applicable.

A weak concave streamline curvature also occurs around the separation location of an LSB. It may give rise to a Görtler instability despite the absence of curved walls. Inger (1987) (1987, p. 1) investigated the 'possibility of an analogous type of mechanism arising locally in separating shear flows.' He derived a parameter based on the strength of streamline curvature at separation. If this parameter exceeds a certain value, 'within the boundary layer above the separation point, spanwise periodic disturbances in the form of contra-rotating streamwise vortex pairs should appear" (Inger 1987, p. 3). He also derived a set of linearized stability equations but without being able to find a solution to them.

From a computation of separated flows, Pauley (1994) (1994, p. 438) concluded that '[v]elocity contours across the channel span showed the formation of Görtler vortices as predicted by Inger (1987) for many conditions producing laminar separation.' Unfortunately, Pauley (1994) does not back this conclusion by e.g. providing evidence of steady, spatially growing three-dimensional disturbances at the separation point. The same is true for a follow-up study (Wilson & Pauley 1998). Both papers only show a plot of instantaneous contours of the spanwise velocity component at a single position deep inside the separation bubble, at which streamlines should have the wrong curvature (convex instead of concave) (cf. figure 9 in Wilson & Pauley 1998 or figure 8 in Pauley 1994).

Thus, there is a need for more conclusive evidence for the appearance of Görtler vortices as predicted by Inger (1987) for separating flows.

1.1.2. *Transient growth*

Research of bypass transition in ZPG boundary layers revealed the possibility of temporal transient growth of steady spanwise disturbances due to non-orthogonality of the eigenmodes (e.g. Trefethen *et al.* 1993; Schmid & Henningson 2001). If the flow is stable, growth in time is bounded by viscosity.

Similarly, spatial transient growth associated with the lift-up effect occurs only for a finite downstream distance. Nevertheless, it can lead to considerable amplitudes. In what follows we will only consider spatial transient growth.

Using adjoint methods, an iteration procedure can be applied to calculate the inflow disturbance resulting in the largest gain in disturbance energy for a certain streamwise distance (Schmid & Henningson 2001). Investigations in boundary layers (Andersson *et al.* 1999; Luchini 2000; Levin & Henningson 2003) show that the optimal disturbance is a steady, spanwise-modulated streamwise vortex that relaxes into a streak downstream. Luchini (2000) pointed out that equations for studies of spatial transient growth are the same as for studies of Görtler instability, except for the absence of a centrifugal term.

The presence of streaks in conjunction with separating flows was experimentally observed by Watmuff (1999). Streak development in such flows and their relation to transient growth has only recently been studied experimentally and theoretically by Boiko (2002). However, we will not just consider the APG region here, since

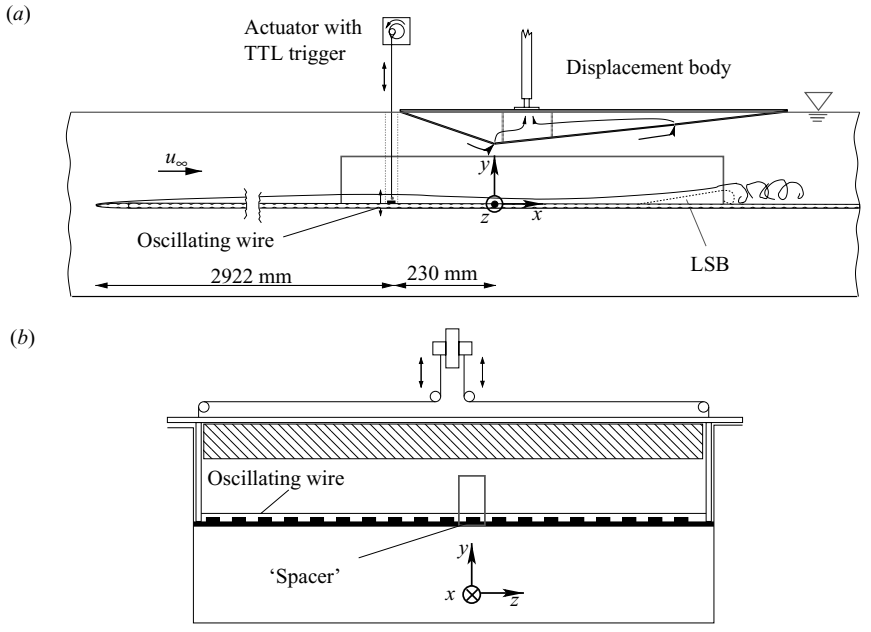

FIGURE 1. Sketch of the test section of the laminar water tunnel at the IAG. The integration domain used for DNS is indicated by a box (not to scale): (*a*) side view; (*b*) front view.

disturbances are often already present upstream of deceleration, as e.g. in the experiments by Watmuff (1999) and Lang *et al.* (2004). Levin *et al.* (2005) showed evidence of steady three-dimensional disturbances in a Blasius wall jet. A wall jet is similar to a separating flow in the sense that it also has a strong instability of the shear layer away from the wall.

In addition to Görtler instability, transient growth is another candidate for the appearance of steady three-dimensional disturbances in separating flows, and neither has been sufficiently explored.

1.2. *Related work and outline*

In this paper, we focus on physical mechanisms leading to steady three-dimensional disturbance growth. Some results supplementing this paper, like a discussion of the shear-layer instability and the influence of the spanwise wavelength of the three-dimensional disturbance, can be found in Marxen *et al.* (2004), Marxen (2005) and Marxen *et al.* (2006). Boiko (2004, personal communication) investigated disturbance evolution in the acceleration region theoretically.

First, the underlying base flow obtained from measurements and direct numerical simulation (DNS) is described (§ 2). Next, details of the forcing of steady three-dimensional disturbances in experiment and DNS are given (§ 3). DNS and measurements for the disturbance evolution are compared with each other (§ 4) and with theoretical results (§ 5) in order to evaluate physical mechanisms leading to disturbance growth. We close with a summary (§ 6).

2. Base flow: time-averaged LSB

A sketch of the experimental set-up is given in figure 1. Only a brief description will be given here; for details the reader is referred to Lang *et al.* (2004) and Lang (2005).

A Cartesian reference system ($\check{x}, \check{y}, \check{z}$), as shown in figure 1, constitutes the basic reference system throughout this work (dimensional quantities are marked by $\check{}$). A velocity vector is denoted as $\boldsymbol{v} = [u, v, w]^T$.

2.1. *Description of the experimental set-up*

A flat plate is mounted in the free stream (free-stream velocity $\check{U}_\infty = 0.125\,\mathrm{m\,s^{-1}}$) of the test section of a laminar water tunnel (turbulence intensity $Tu \leqslant 0.05\,\%$ for 0.1–10 Hz at $0.145\,\mathrm{m\,s^{-1}}$). A streamwise pressure gradient is imposed locally on the flat-plate boundary layer by a displacement body with a length $\check{L}_{DB}^{Exp} = 0.69\,\mathrm{m}$, inducing an FPG region followed by an APG. In the region of the APG (starting at $\check{x} \approx 0\,\mathrm{m}$), an LSB develops. The reference length is chosen to be $\check{L}_{ref}^{Exp} = 2/3\ \mathrm{m} \approx \check{L}_{DB}^{Exp}$. The reference velocity (for its derivation see Marxen 2005) amounts to $\check{U}_{ref}^{Exp} = 0.151\ \mathrm{m\ s^{-1}} \approx 1.2\check{U}_\infty$, resulting in a Reynolds number $Re_{global} = \check{U}_{ref}^{Exp}\check{L}_{ref}^{Exp}/\check{\nu} = 10^5$.

The set-up was used during several measurement campaigns carried out at the Institut für Aerodynamik und Gasdynamik (IAG), Universität Stuttgart. Data of these campaigns will be used for comparison with computational results throughout this paper. Specifically, results from measurements by means of laser-Doppler anemometry (LDA) in 2000 and 2001 are used, denoted below as 'LDA (2000)' and 'LDA (2001)', respectively.

Transition occurs in the detached shear layer even without any forcing: vortex shedding is followed by an immediate breakdown to three-dimensional small-scale structures. Rist & Augustin (2006) have demonstrated the high sensitivity of an LSB to forcing at a frequency which is strongly amplified by the shear layer. To ensure reproducible results that are independent of this particular water tunnel and its background noise in the relevant frequency range and to allow for a phase-averaged post-processing, it is desirable to control the disturbance spectrum in the flow. Following a classic approach in transition research (Klebanoff, Tidstrom & Sargent 1962; Kachanov & Levchenko 1984), this is achieved by forcing disturbances explicitly by means of an oscillating wire and spacers (see § 3.1).

As the steady three-dimensional disturbances are spanwise periodic and evolve linearly, there is no conceptual difference between forcing them in the form of a fixed spanwise spacing (as done here), forcing a (stationary) local wave packet or forcing these disturbances in some presumably natural way.

2.2. *DNS to obtain the base flow for investigations of disturbance evolution*

To obtain a base flow for subsequent disturbance investigations, a DNS with controlled disturbance input had to be carried out. This DNS provided an LSB close in shape to the experimental one. For DNS calculations, general physical parameters of the flow have been chosen to match the flow field resulting from the experimental set-up (§ 2.1) as accurately as possible. The incompressible three-dimensional Navier–Stokes equations in vorticity–velocity formulation are solved using a high-order method (Kloker 1998).

At the inflow boundary, a self-similar laminar boundary-layer profile is prescribed. A favourable-to-adverse pressure gradient is induced via the streamwise velocity at the upper boundary. At the outflow, a buffer zone returns the flow to a steady laminar state so that perturbations can leave the domain without being reflected. Explicit disturbance forcing via wall blowing and suction models the experimental disturbance input. For details and a reasoning for the choice of the boundary conditions, in particular with respect to the upper boundary, see Marxen (2005), where it is denoted as the case D_{NLDE}.

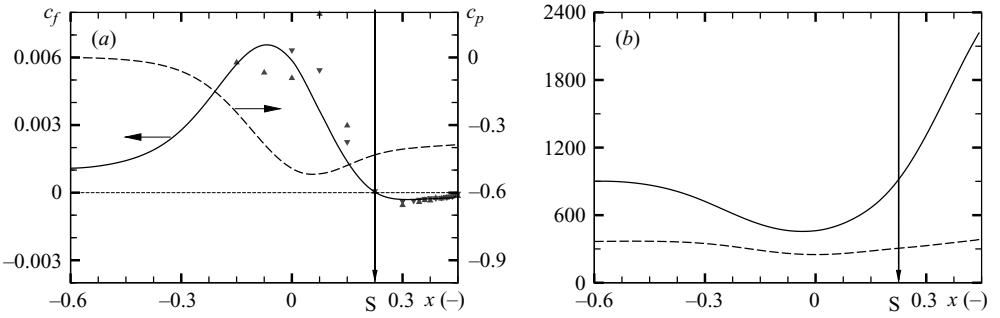

FIGURE 2. (*a*) Coefficients for surface pressure c_p (dashed line), skin friction c_f (solid line); (*b*) Reynolds numbers Re_{δ_1} (solid line) and Re_{δ_2} (dashed line). Lines denote DNS, and symbols denote LDA (2000) and LDA (2001); c_f has been computed from wall-normal derivatives of measured profiles of the streamwise mean velocity.

The mean flow is obtained by averaging DNS results over time and span. The start of the separation bubble is marked by the point of separation S. Boundary-layer quantities from DNS, like displacement thickness δ_1 and momentum thickness δ_2, are computed from a wall-normal integration of the spanwise vorticity $\omega_z = \partial u/\partial y - \partial v/\partial x$ (Spalart & Strelets 2000):

$$Re_{\delta_1} = u_{psd}(y_{max}) \times \delta_1 \times Re_{global}, \quad Re_{\delta_2} = u_{psd}(y_{max}) \times \delta_2 \times Re_{global}, \tag{2.1}$$

$$\text{with } u_{psd}(y) = \int_0^y \omega_z(s)\,\mathrm{d}s, \tag{2.2}$$

$$\delta_1 = \int_0^{y_{max}} \left(1 - \frac{u_{psd}(s)}{u_{psd}(y_{max})}\right) \mathrm{d}s, \tag{2.3}$$

$$\delta_2 = \int_0^{y_{max}} \frac{u_{psd}(s)}{u_{psd}(y_{max})} \left(1 - \frac{u_{psd}(s)}{u_{psd}(y_{max})}\right) \mathrm{d}s. \tag{2.4}$$

In these equations, y_{max} denotes the height of the integration domain used in the computation. However, results are independent of the value of y_{max} as long as it lies in the region of vanishing vorticity, i.e. outside the boundary layer. Coefficients for surface pressure c_p and skin friction c_f are computed from

$$c_p = 2 \int_0^x \left.\frac{\partial^2 u(s)}{\partial y^2}\right|_{y=0} \mathrm{d}s, \tag{2.5}$$

$$c_f = 2\ \omega_z|_{y=0} / Re_{global}. \tag{2.6}$$

Figure 2 shows the streamwise development of these boundary-layer quantities.

The time- and spanwise-averaged flow field upstream of transition can be considered as a good approximation to the steady Navier–Stokes equations. Up to a streamwise position of $x = 0.3$, velocity disturbance amplitudes remain below 10^{-3}. Their possible direct contribution to the base flow due to nonlinear interaction is therefore roughly of the order of 10^{-6}. At $x = 0.42$, this direct contribution has risen to 10^{-4}.

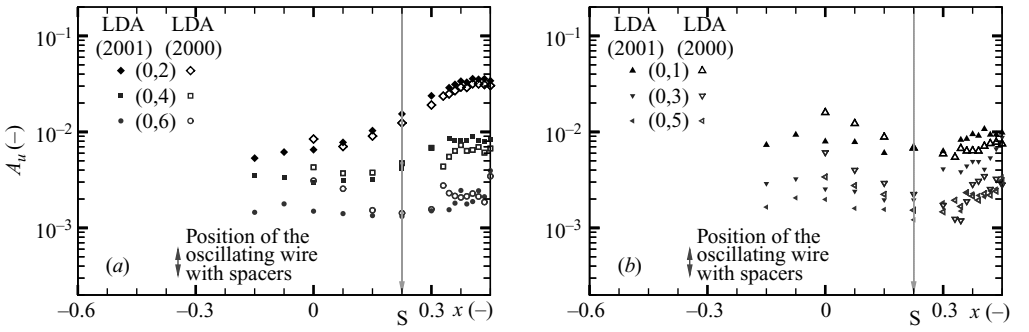

FIGURE 3. Amplification curves for the maximum (in y) steady streamwise velocity fluctuation $A_u = |\hat{u}'^{(0,k)}|_{max}$: (*a*) even modes $k = 2, \ldots, 6$; (*b*) odd modes $k = 1, \ldots, 5$. Filled symbols denote LDA (2001), open symbols denote LDA (2000).

3. Investigating the disturbance evolution in experiment and DNS

DNS results presented below were obtained using a disturbance-flow formulation. In this formulation, a laminar flow is assumed to fulfil the steady Navier–Stokes equations and is used as a base flow. A solution is then sought only for the disturbance quantities $\boldsymbol{v}'$, $\boldsymbol{\omega}'$. As a base flow $\boldsymbol{v}_B$, $\boldsymbol{\omega}_B$, the mean flow described in § 2.2 was used. The advantage of using a disturbance formulation is a drastically reduced computational cost due to shorter integration domains, lower spanwise resolution requirements and much shorter convergence times towards a periodic or steady state (see Marxen *et al.* 2004).

For simulations in disturbance-flow formulation we consider only the first, i.e. laminar, part of the LSB (box in figure 1). The numerical method is the same as in § 2.2. However, a different set of boundary conditions was applied, namely exponential decay of velocity disturbances at the upper boundary. The flow field in the DNS is periodic in spanwise direction and symmetric with respect to a plane $z = 0$.

All results are Fourier analysed in time and the spanwise direction. Fourier coefficients will be marked by $\hat{}$ and amplitudes by $|\hat{}|$ or A. The notation (h, k) will be used here to denote modes with h times the fundamental frequency $\beta_0 = 2\pi f_0$ and k times the spanwise wavenumber $\gamma_0 = 2\pi/\lambda_z$.

3.1. *Disturbance forcing in the experiment*

A two-dimensional time-harmonic disturbance is introduced upstream of the displacement body at $\breve{x} = -0.23$ m ($x = -0.345$) by an oscillating wire of frequency $\breve{f}_0 = 1.1$ Hz. Additionally, three-dimensional disturbances are imposed by placing thin (height 10^{-3} m) metal plates (the so-called spacers, figure 1) regularly underneath the wire. Their spacing gives the fundamental spanwise wavelength $\breve{\lambda}_z = 0.058$ m. LDA data were phase-averaged using a transistor–transistor logic (TTL) trigger signal generated by the actuator driving the wire (Lang *et al.* 2004).

Although several different spanwise harmonics are excited by the spacers, mode (0, 2) is the largest disturbance in the first part of the LSB (figure 3). It is even larger than any unsteady disturbance (h, k) with non-zero h. Thus, focus will only be put on the behaviour of this mode. The set-up in the LDA (2000) and LDA (2001) cases differs slightly in the wall-normal position of the oscillating wire, which explains the slightly different amplitudes as visible in figure 3.

Case	(0, 1)	(0, 2)	(1, 0)	(1, ±1), each	(1, ±2), each	End of useful region $x \approx$
B_{01}	0.200	–	–	–	–	> 0.33
B_{02}	–	0.145	–	–	–	> 0.33
$B_{10,12}$	–	–	1.000	–	0.500	> 0.33
B_{11}	–	–	–	0.335	–	> 0.33
B^{11}	–	–	–	1.12	–	> 0.39

TABLE 1. Disturbance v-amplitudes A_v, given in percent (or $\times 10^{-2}$), for all cases ($\beta_0 = 30.7$, $\gamma_0 = 72.0$).

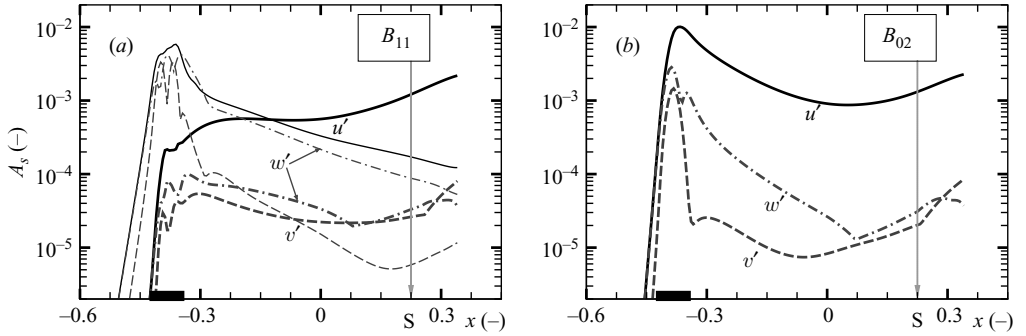

FIGURE 4. Amplification curves for the maximum (in y) streamwise (solid line), wall-normal (dashed line) and spanwise (dash-dotted line) velocity fluctuation $A_s = |\hat{s}'^{(h,k)}|_{max}$. (*a*) Modes (1, 1) (thin line), (0, 2) (thick line) of case B_{11}. (*b*) Mode (0, 2) (thick line) of case B_{02}.

3.2. *Disturbance forcing in DNS: direct excitation versus nonlinear generation*

The choice of the location for disturbance input in DNS is roughly guided by the experiment. Disturbances in DNS are locally forced via zero net mass flux (at every instant) blowing/suction at the wall in the region $x \in [-0.4268, -0.3398]$. In the following figures, the disturbance strip is visualized by a bar within the x-axis.

The disturbance amplitudes of the wall-normal velocity A_v for the different DNS cases are given in table 1. Nomenclature for the denotation of the cases follows the one introduced in Marxen *et al.* (2004). Indices refer to multiples of the fundamental frequency (first digit), multiples of the spanwise wavenumber (second digit) and amplitude level (superscript = high level, subscript = low level) of the disturbance input. For instance, in case B_{01} a steady three-dimensional disturbance is forced with $h = 0$ and $k = 1$ with a low amplitude level. In case $B_{10,12}$ more than one disturbance was forced.

Only case B_{02} corresponds to direct disturbance excitation of mode (0, 2), while in all other cases mode (0, 2) is a result of nonlinear generation. In all cases no continuous forcing of steady disturbances occurs, as they are independent of their origin already slightly downstream of the disturbance strip from $x \approx -0.3$ onwards.

The acceleration region which damps out unsteady fluctuations in particular (figure 4*a*), prevents continuous nonlinear generation. A comparison with the experiment will follow in figure 5.

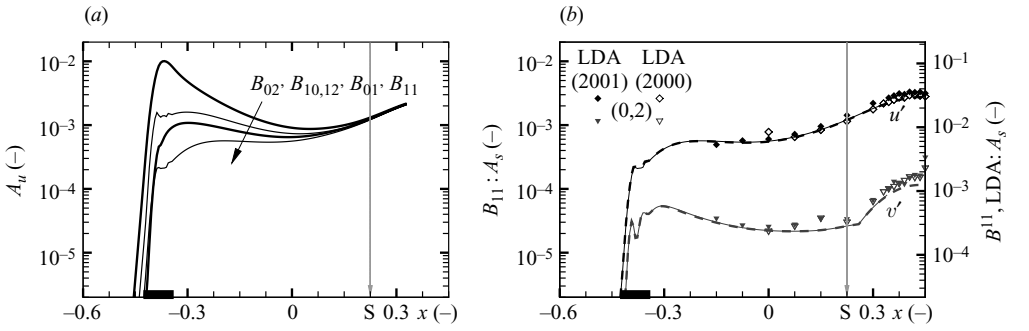

FIGURE 5. Same as figure 4, except only $|\hat{u}'|$, $|\hat{v}'|$ are shown. (*a*) Modes (0, 2) of cases B_{xx}: B_{01}, B_{02} (thick lines) and B_{11}, $B_{10,12}$ (thin lines). (*b*) Modes (0, 2) of cases B_{11} (solid line) and B^{11} (dashed line) as well as LDA (2001) (filled symbols) and LDA (2000) (open symbols). Note the different axis scalings of the ordinate: left B_{11}, right B^{11} and LDA.

4. Results from DNS and measurements

First, disturbances in the FPG region are investigated (§ 4.1). Main emphasis, however, is put on the APG region and the first part of the LSB (§§ 4.2 and 4.3).

4.1. *Lift-up effect and transient growth upstream of separation*

The low-amplitude cases B_{xx} (table 1) will be compared with respect to the streamwise evolution of mode (0, 2) in the interval $x \in [-0.3, 0.075)$ (e.g. thick lines in figure 4). This interval lies within the FPG region. We observed (not shown here) that all cases possess a different ratio $|\hat{u}'|_{max} : |\hat{v}'|_{max} : |\hat{w}'|_{max}$. For an easier comparison, forcing amplitudes have been chosen such that all four cases possess the same amplitudes downstream of separation S (figure 5*a*).

All cases exhibit (stronger or weaker) signatures of the lift-up effect. In a parallel mean flow, the lift-up effect can cause the disturbance component in the mean-flow direction to grow if a disturbance component perpendicular to the mean shear is present. This implies that in a stable parallel flow, no growth should be visible in $|\hat{v}'|$.

In the FPG region, we do not observe a growing $|\hat{v}'|$ (figure 4) even though the flow is not exactly parallel. Apparently, v_B is sufficiently small.

The development of $|\hat{u}'|$ is governed by a competition between growth due to lift-up and viscous decay. If a large $|\hat{u}'|$ is present initially, the viscous decay is stronger than the production, or growth, caused by the lift-up effect (case B_{02}, figure 4*b*). In case B_{11}, $|\hat{u}'|$ is initially (i.e. at $x = -0.3$) so small that it increases within the interval $x \in [-0.3, -0.225]$, while both $|\hat{v}'|$ and $|\hat{w}'|$ decrease (figure 4*a*): the lift-up effect has caused transient growth.

The cases B_{01} and $B_{10,12}$ lie in between the cases B_{02} and B_{11}: the lift-up effect is still visible via an increasing quotient $|\hat{u}'|_{max}/|\hat{v}'|_{max}$, but it is not sufficiently strong to cause $|\hat{u}'|$-disturbance growth downstream of $x = -0.3$.

All cases B_{xx} possess a disturbance level lower than that observed experimentally. To allow for a proper comparison with measurements, case B^{11} with increased excitation amplitude was computed. This case favourably compares with experimentally determined amplitudes (figure 5*b*). Moreover, figure 5(*b*) proves that the disturbance evolution in cases B_{11} and B^{11} is indeed linear, i.e. independent of absolute amplitude. For that reason, we will no longer specifically distinguish between cases B_{11} and B^{11} below.

It is remarkable how similar respective $|\hat{u}'|$-amplitude functions $A_u = |\hat{u}'(y)|$ look for all cases in the interval $x \in [-0.3, 0.075)$ (figure 6), no matter whether transient growth occurred (case B_{11}) or not (case B_{02}). On the other hand, this similarity becomes understandable if we recognize that $\hat{u}'$ is a result of lift-up in all cases. In case B_{11} the lift-up effect occurs continuously along x and is responsible for transient growth (figure 4*a*). Instead, in case B_{02} it occurs only for the disturbance-strip region (figure 4*b*).

Slightly downstream of $x = -0.15$ transient growth has vanished even in case B_{11}. At this point, $|\hat{u}'|$ has become more than an order of magnitude larger than $|\hat{v}'|$ or $|\hat{w}'|$. For that reason, we can denote the disturbance as a u'-streak.

The overall disturbance shape in the streak region ($x > -0.15$) is similar to that known from Görtler instability, where it is usually called a streamwise vortex despite $|\hat{u}'| = O(\sqrt{Re} \cdot |\hat{v}'|) \gg |\hat{v}'|$.

Case B^{11} shows the best overall agreement with experimental results already in the FPG region ($x \lesssim 0$). This is true with respect to amplification (figure 5*b*) as well as disturbance shape (figure 6). Thus, steady disturbances observed in the experiment are a result of nonlinear generation caused by a fluctuating disturbance mode (1, 1). Further justification for this hypothesis can be found in Marxen *et al.* (2004): they found that case B^{11} agrees perfectly with the experiment – not only with respect to the steady perturbations but also for the unsteady perturbations.

4.2. *Generic (modal) growth in the APG region*

In the region $x \in [0.075, 0.225]$ differences between the cases B_{xx} gradually decrease (figure 7). All cases come together at roughly the same x-position: at separation S ($x = 0.225$), deviation in disturbance growth (figure 5*a*) and shape (figure 7, lower panels) has become negligible. We will argue that the disturbance evolution in this region cannot solely be explained by transient growth (due to the lift-up effect) as in the FPG region. Instead, evidence is presented that modal growth occurs in the APG region. A physical mechanism causing the instability will be suggested in § 5.

In this and the next paragraph, we mainly consider case B_{11} or B^{11} within $x \in [-0.15, 0.39]$. This case agrees best with measurements, and it will turn out that this case is closest to pure modal growth, too.

Modal growth implies that a single, common growth rate can be defined for all velocity components. Even though this can be fulfilled only approximately in non-parallel flow, growth rates based on the different components should still be reasonably close.

A modal growth rate based on following absolute wall-normal maxima (dotted lines in figure 8) fails to meet this criterion. A definition based on total kinetic disturbance energy (which is dominated by $\hat{u}'$) does not appear helpful either, since it cannot distinguish between transient and modal growths.

It is more useful to distinguish between inner and outer maxima (in y) of $|\hat{v}'|$ and $|\hat{w}'|$: Both outer maxima $|\hat{v}'|_{outer}$, $|\hat{w}'|_{outer}$ have at least a qualitatively similar behaviour (figure 8*a*). The slope of $|\hat{v}'|_{outer}$ is still different from the one of $|\hat{u}'|_{max}$ and $|\hat{w}'|_{outer}$. Interestingly, both inner maxima $|\hat{v}'|_{inner}$ and $|\hat{w}'|_{inner}$ (figure 8*b*) grow together around the separation location (for details of this aspect see § 5.3.2).

The qualitatively different evolution of inner and outer $|\hat{v}'|$-disturbance maxima leads to the idea described in the following: While a modal instability amplifies each component of the disturbance vector by the same factor, transient growth (as a result of a lift-up mechanism) acts strongest on those disturbance components which have the largest mean-flow counterpart. Therefore, if the disturbance velocity vector is not

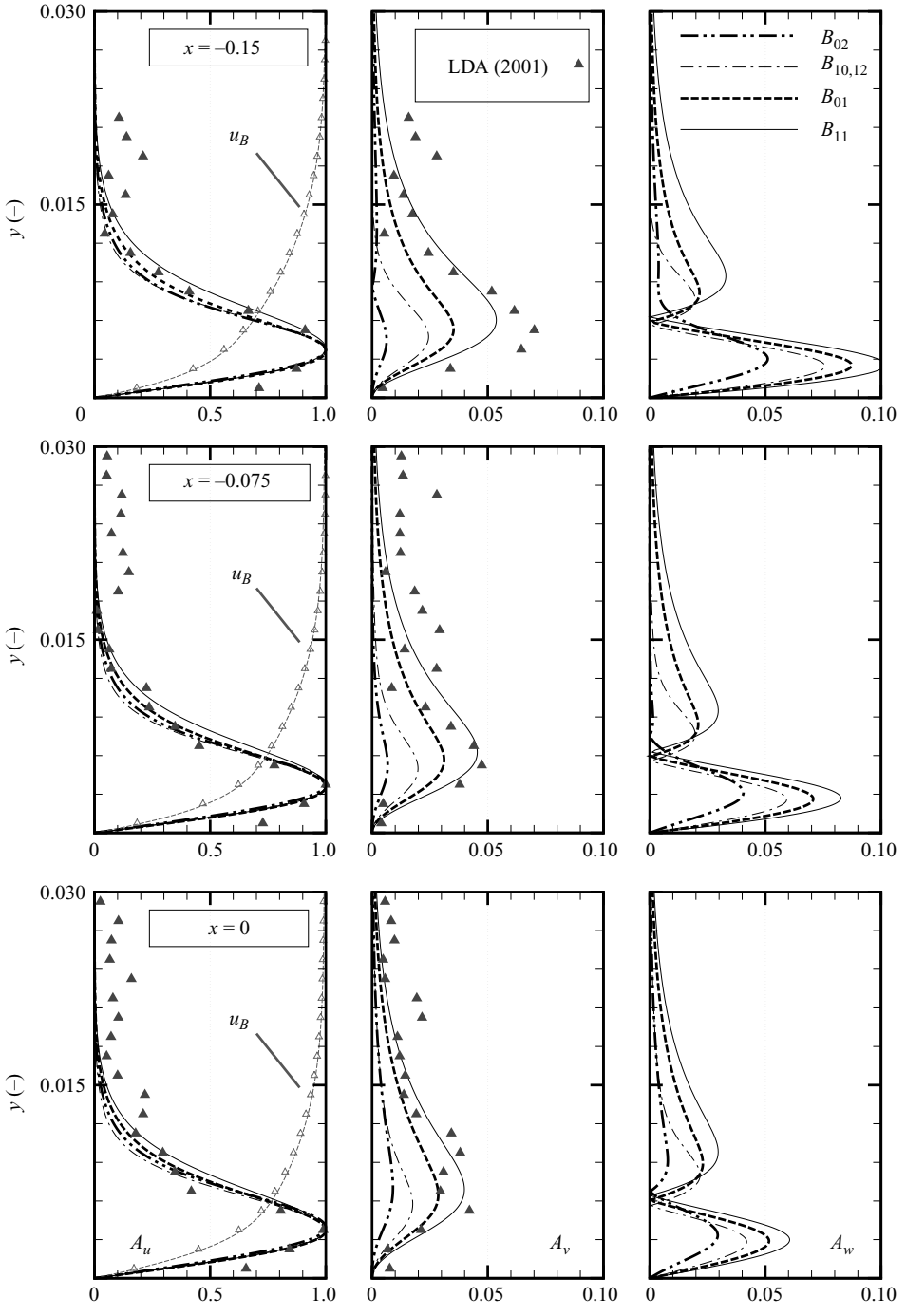

FIGURE 6. Velocity amplitudes of mode (0, 2), normalized by the respective $|\hat{u}'|_{max}$. Comparison of results for cases B_{xx} with measurements in the FPG region for $x = -0.15, -0.075, 0$ (DNS: lines; experiment: symbols). Base-flow quantities u_B are also shown.

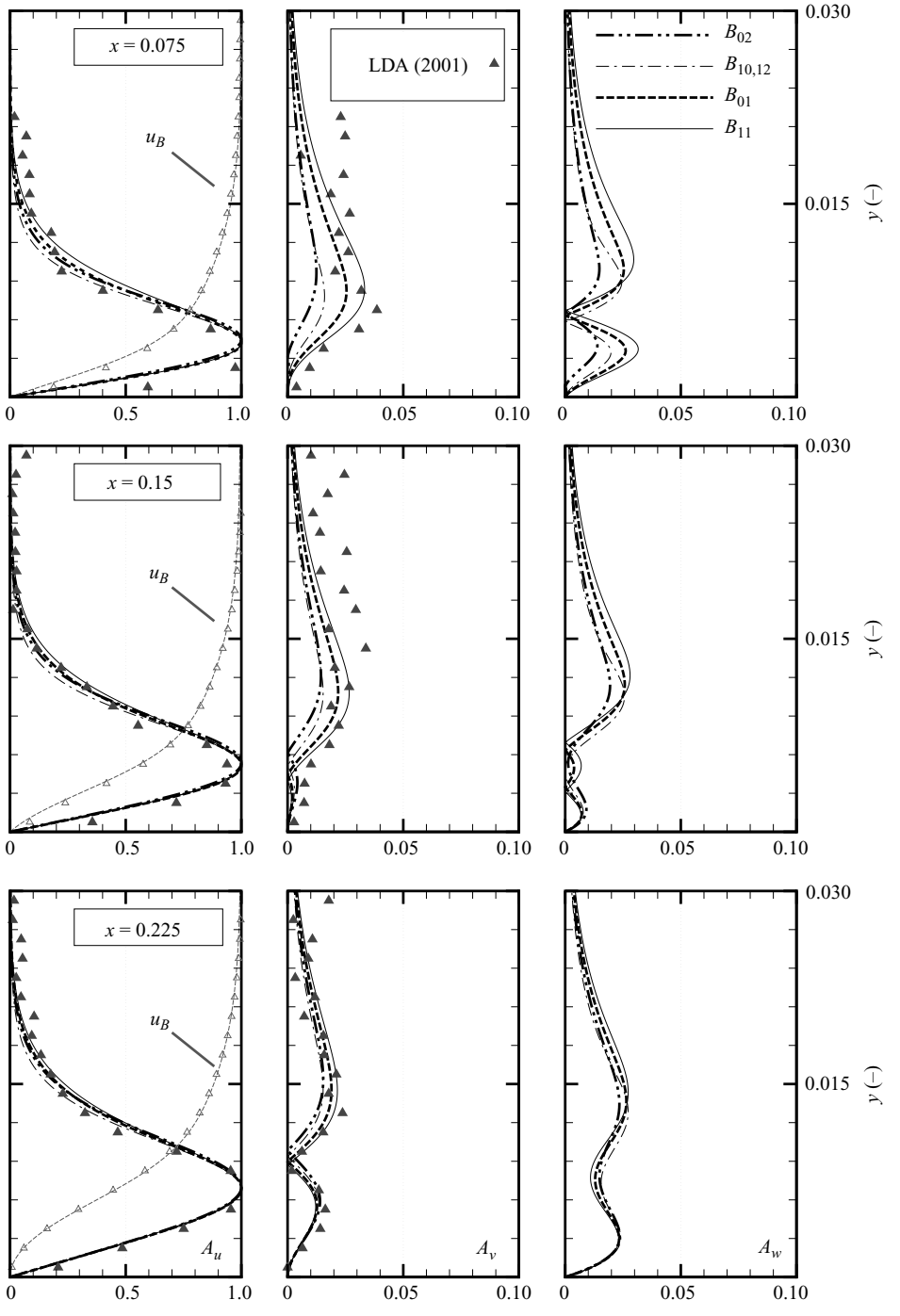

FIGURE 7. Same as figure 6. Comparison of results for cases B_{xx} with measurements in the APG region for $x = 0.075$, 0.15, 0.225 (S). Base-flow quantities u_B are also shown.

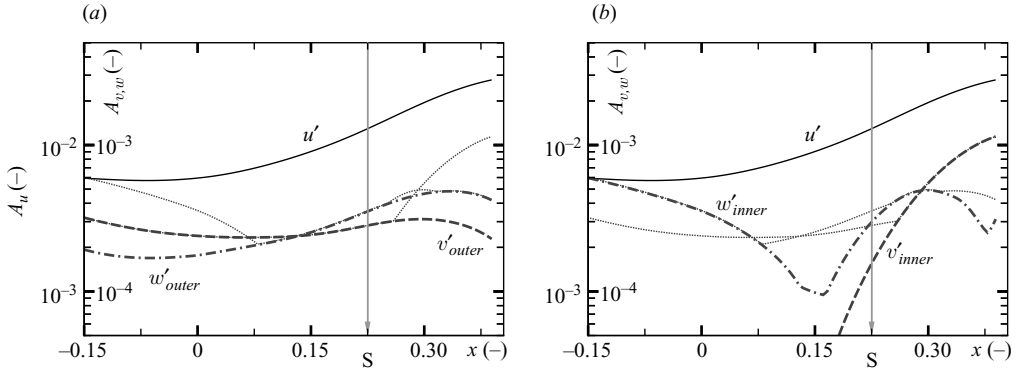

FIGURE 8. Amplification curves from DNS for (local) maximum (in y) velocity fluctuation $|\hat{s}'^{(0,2)}|$ of case B^{11}. (*a*) Outer and (*b*) inner maxima are being followed separately. Evolution of total wall-normal maxima $|\hat{s}'^{(0,2)}|_{max}$ is given as dotted lines for reference.

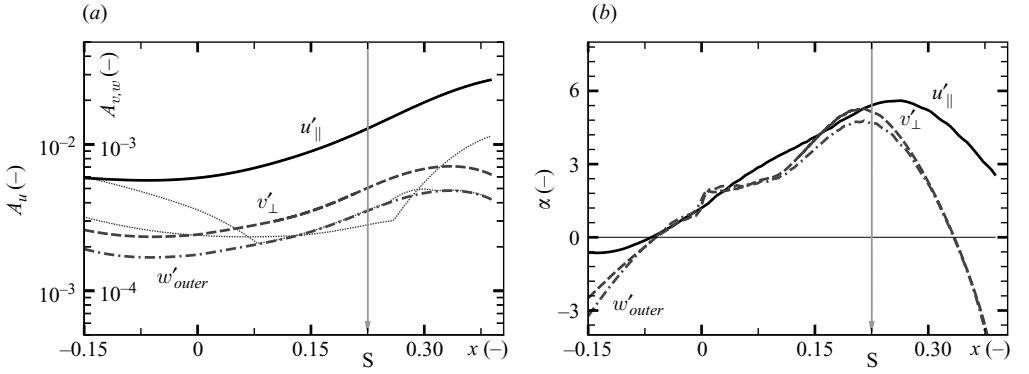

FIGURE 9. (*a*) Wall-normal maxima $|\hat{u}'_{\parallel}|_{max}$, $|\hat{v}'_{\perp}|_{max}$, $|\hat{w}'|_{outer}$ from $|\hat{s}'^{(0,2)}|$ of case B^{11}. Evolution of total maxima $|\hat{s}'^{(0,2)}|_{max}$ is given as dotted lines for reference. (*b*) Corresponding growth rates $\alpha = 1/|\hat{s}'|_{max(or\ outer)} \times \partial|\hat{s}'|_{max(or\ outer)}/\partial x$.

aligned with the base-flow vector in the beginning, it will eventually become aligned in case of transient growth. In turn, if it keeps its angle with respect to the (changing) base flow while growing, this growth should be due to a modal instability. We note that the lift-up effect is not the only mechanism that can lead to transient growth, but it is expected to be particularly important in a boundary layer and even more so in a free shear layer. Levin *et al.* (2005) noted that the transient growth is about 10 times larger for the Blasius wall jet than for a Blasius boundary layer. This effect shall therefore be examined more closely. We introduce the following transformation:

$$[\hat{u}'_{\parallel}\ \hat{v}'_{\perp}\ \hat{w}']^T = \frac{1}{\|\ \boldsymbol{v}_B\ \|} \begin{bmatrix} u_B & v_B & 0 \\ -v_B & u_B & 0 \\ 0 & 0 & \|\ \boldsymbol{v}_B\ \| \end{bmatrix} [\hat{u}'\ \hat{v}'\ \hat{w}']^T. \tag{4.1}$$

The purpose of (4.1) is to follow $\hat{v}'_{\perp}$ along the detaching shear layer, and therefore $\hat{v}'_{\perp}$ is not considered (or equivalently set to zero) in the region below the separating streamline. Wall-normal amplitude maxima of the components of the left-hand-side vector of (4.1) are given in figure 9(*a*). Except where mean reverse flow occurs ($x > 0.225$), both $|\hat{u}'_{\parallel}|$ and $|\hat{v}'_{\perp}|$ possess a single wall-normal maximum only. While

$\hat{u}'_{\parallel}$ cannot be distinguished from $\hat{u}'$, $\hat{v}'_{\perp}$ differs considerably from $\hat{v}'$. Moreover, the lines for $|\hat{v}'_{\perp}|_{max}$ and $|\hat{w}'|_{outer}$ in figure 9(*a*) would (almost) collapse if shifted by a constant.

The difference between $|\hat{v}'_{\perp}|_{max}$ and $|\hat{v}'|_{max}$ can roughly be explained as follows: For the strong FPG at $x<0$, the base-flow vector points slightly towards the wall ($v_B<0$). Thus, in (4.1) a positive $\hat{u}'$ gives a small positive contribution to (the negative) $\hat{v}'_{\perp}$, so that $|\hat{v}'_{\perp}|<|\hat{v}'|$ (figure 9*a*). The opposite is true in the APG region, $x>0$. This argument is supported by the favourable correlation between the slope of Re_{δ_1} (figure 2*b*) and the difference $|\hat{v}'_{\perp}|_{max}-|\hat{v}'|_{max}$ in the region $x\in[-0.15, 0.225]$.

The growth rates $\alpha=1/|\hat{s}'|\cdot\partial|\hat{s}'|/\partial x$ (figure 9*b*) are small first but continuously increase until a maximum is reached close to S. Most importantly, now all three components exhibit essentially the same growth rate. This can be interpreted as the disturbance vector roughly keeping its shape relative to the mean-flow vector while growing. It indicates the existence of a single (amplified) eigenmode. In fact, this shape argument largely holds for $\hat{u}'_{\parallel}$ and $\hat{v}'_{\perp}$ if we account for boundary-layer growth by normalizing the y-coordinate with δ_1 (for $\hat{u}'$ see Marxen 2005, and for $\hat{v}'_{\perp}$ see figure 17 below). Justification to use $|\hat{w}'|_{outer}$ when computing growth rates comes from the fact that the instability takes place away from the wall, following the separating shear layer, as is later explained in § 5.2 and § 5.3.2.

4.3. *Transient effects in the APG region*

4.3.1. *Disturbance evolution deeper inside the separation bule: transient growth*

Downstream of S transient growth sets in again, despite the persistence of a modal instability: a larger growth rate in $|\hat{u}'|$ compared to $|\hat{v}'_{\perp}|$ and $|\hat{w}'|_{outer}$ is seen (figure 9*b*). In turn, this suggests that the disturbance can now be regarded as a superposition of modes again. Since all components are still growing, we have a mixture of transient and modal growths.

Deeper inside the LSB ($x>0.33$), $|u'_{\parallel}|$ continues to grow, while $|\hat{v}'_{\perp}|$ and $|\hat{w}'|$ decay (figure 9*a*). Thus, downstream of the modal-instability region we have again a region of transient growth. It is the parallel component ($\hat{u}'_{\parallel}$) which grows due to the lift-up effect. This explains why we observe growth in $|\hat{u}'|$ and $|\hat{v}'|$.

4.3.2. *Additional transient effects in the region of modal growth*

In § 4.2, we have presented strong evidence that disturbance evolution in case B_{11}/B^{11} up to S is purely due to a modal instability with common amplification rates, no matter if based on $|\hat{u}'_{\parallel}|$, $|\hat{v}'_{\perp}|$, or $|\hat{w}'|_{outer}$. It turns out that case B_{01} is close to case B_{11} (or B^{11}) and will therefore not be considered further.

However, in cases B_{02} and $B_{10,12}$, larger growth can be observed in $|\hat{v}'_{\perp}|$ (and in case B_{02} also in $|\hat{w}'_{outer}|$) but smaller growth in $|\hat{u}'_{\parallel}|$ (figure 10). In fact, one may say the following: the smaller the growth rate of $|\hat{u}'_{\parallel}|$, the larger the growth of $|\hat{v}'_{\perp}|$. An explanation is the occurrence of transient growth for the entire domain, which – within the unstable region – occurs simultaneously with the modal growth. The (assumed) superposition of amplified and damped modes is such that $|\hat{v}'_{\perp}|$ and $|\hat{w}'|$ grow stronger than modal, while $|\hat{u}'_{\parallel}|$ grows weaker.

5. Physical mechanisms of the disturbance growth

A theoretical method is applied to the present flow. It is based on the linearized boundary-layer equations and seeks a general solution by means of an optimization

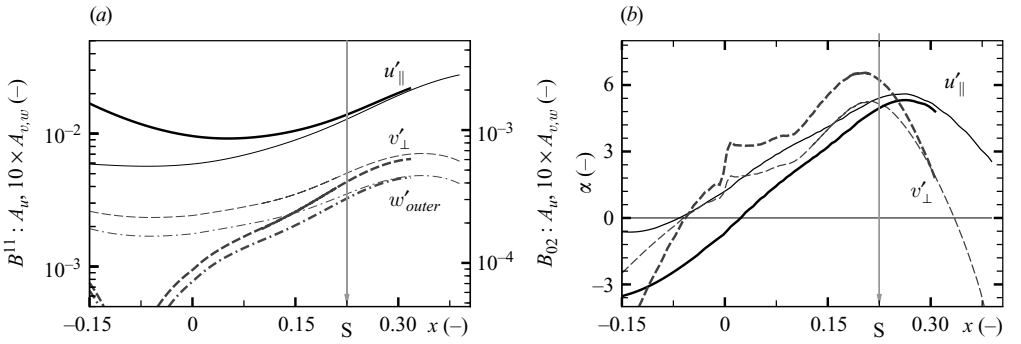

FIGURE 10. Same as figure 9. (*a*) Case B_{02} (thick lines) versus B^{11} (thin lines). (*b*) Case $B_{10,12}$ (thick lines) versus B^{11} (thin lines).

procedure. The purpose of applying this method is threefold. First, it will give an upper bound to the disturbance growth. Second, a comparison to DNS results will help to understand the dynamics of the disturbance evolution in the FPG region by means of the identification of similarities and differences. Third, if a modal instability is present in the APG region sufficiently far downstream of the forcing (i.e. inflow) location in the theory, we expect to see disturbance growth. Observing such a growing disturbance with the same growth rate independent of the inflow location can therefore be regarded as additional evidence for the occurrence of a modal instability (§ 5.1). In order to evaluate the cause of the onset of modal growth, we define an equivalent Görtler number (§ 5.2). Finally, the evolution of the wall-normal amplitude functions in the non-parallel and separating flow will be discussed (§ 5.3).

5.1. *Spatial optimal growth based on the linearized boundary-layer equations*

The theoretical method utilizes an adjoint-based algorithm to optimize the inflow disturbance profile at x_0 in order to obtain the largest disturbance energy at the outflow position x_1. Details of the method can be found in Andersson *et al.* (1999) and Levin & Henningson (2003). It is known to be valid in attached boundary layers but has not yet been applied to separated flows.

The base flow comes from DNS and was interpolated on to the grid used in the boundary-layer equations. Five different streamwise stations were taken as the inflow position ($x_0 = -0.6, -0.45, -0.3, -0.15, 0$). The outflow position was kept fixed at $x_1 = 0.3348$.

5.1.1. *Optimally growing disturbances in the FPG region*

The amplification of $\hat{u}'$ for all inflow positions x_0 are compared with DNS results in figure 11(*a*). The best agreement in the interval $x \in [-0.6, -0.075]$ of theoretical results with DNS is seen in case B^{11}, which was the case in which we observed a transiently growing $|\hat{u}'|$ within $x \in [-0.3, -0.225]$. The agreement is particularly good if x_0 lies at a similar location or upstream of the disturbance strip in DNS (i.e. $x_0 = -0.6$ or -0.45). Hence, for a further comparison with the DNS we choose case B^{11} and the optimal disturbance prescribed at $x_0 = -0.45$ (figure 11*b*).

The theoretically obtained disturbance is initially a pure streamwise vortex ($\hat{u}' = 0$ at $x = x_0$). It decays, while the lift-up effect induces a strong transient $|\hat{u}'|$-growth, so that eventually $|\hat{u}'| \gg |\hat{v}'|, |\hat{w}'|$. The final outcome is a u'-streak. This sequence of processes is analogous to that in a ZPG boundary layer (Andersson *et al.* 1999).

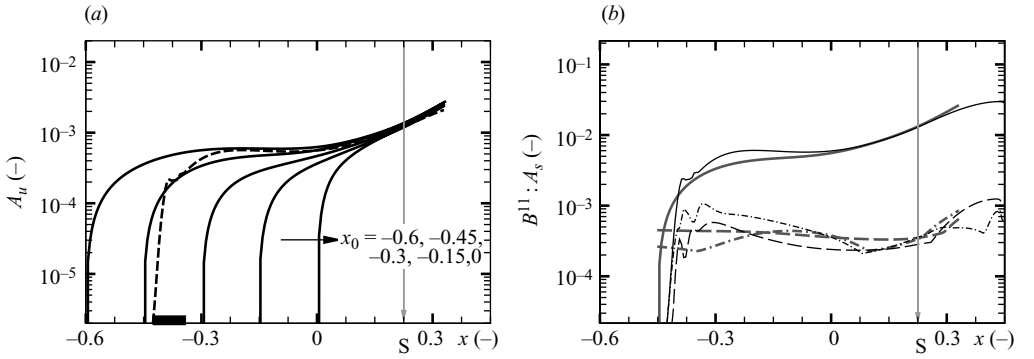

FIGURE 11. Amplification curves for the maximum (in y) velocity fluctuation $|\hat{s}'^{(0,2)}|_{max}$. (a) DNS case B_{11} (dashed line) and optimal perturbations for $x_0 = -0.6, -0.45, -0.3, -0.15, 0$ (thick lines); (b) DNS for case B^{11} (thin lines) and optimal perturbation for $x_0 = -0.45$ (thick lines): streamwise (solid line), wall-normal (dashed line) and spanwise (dash-dotted line) components.

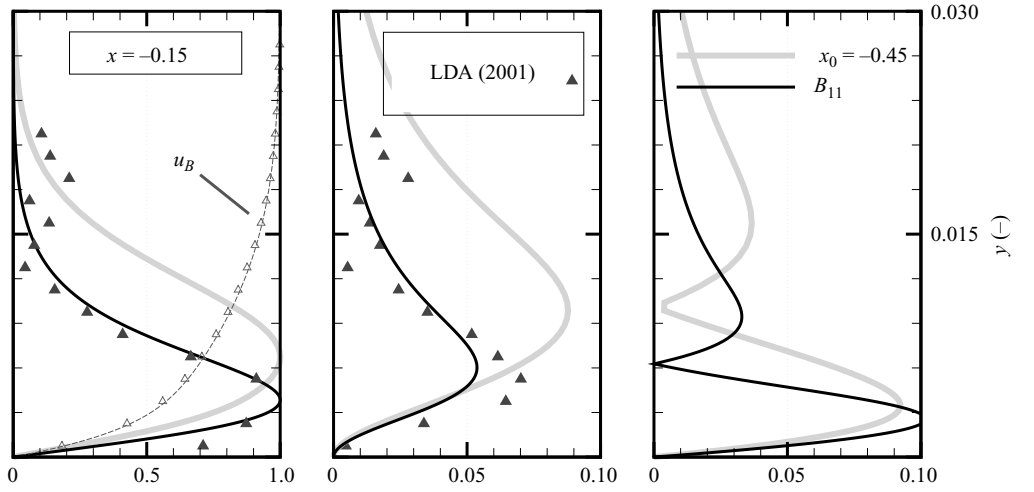

FIGURE 12. Velocity amplitudes of mode (0, 2), normalized by the respective $|\hat{u}'|_{max}$. Comparison of results for $x = -0.15$ from DNS (B^{11}, thin lines) and optimal perturbations ($x_0 = -0.45$, grey lines) with measurements (symbols).

Due to a weaker streamwise decay of $|\hat{v}'|$ in the boundary-layer computations, the growth in $|\hat{u}'|$ is stronger than in the DNS and never vanishes for any x (figure 11b). Responsible for this effect is the difference in wall-normal disturbance functions $\hat{v}'$ (figure 12).

5.1.2. *Optimal growth versus optimal wall-forcing: a comment on receptivity*

The non-normal nature of the local stability operator leads to both transient growth and sensitivity to forcing (for details see Schmid & Henningson 2001). This gives an indication as to why none of the DNS cases nor the experiment agrees perfectly with the optimal calculations (figure 11b). While the shape of the amplitude functions is qualitatively the same, the optimal position for forcing (i.e. maximum $\hat{v}'$ at the inflow) is further away from the wall (figure 12). However, the disturbance excitation takes

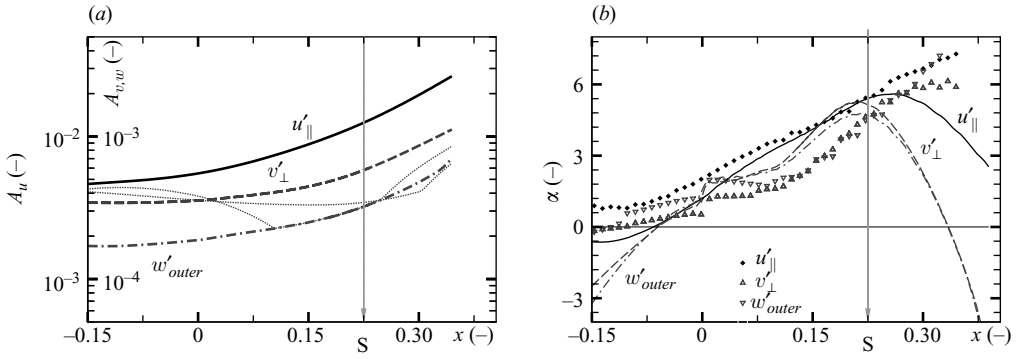

FIGURE 13. (*a*) Wall-normal maxima $|\hat{u}'_{\parallel}|_{max}$, $|\hat{v}'_{\perp}|_{max}$, $|\hat{w}'|_{outer}$ from theoretical case $x_0 = -0.45$. Total wall-normal maxima $|\hat{u}'|_{max}$, $|\hat{v}'|_{max}$, $|\hat{w}'|_{max}$ are given as dotted lines. (*b*) Corresponding growth rates $\alpha = 1/|\hat{s}'| \times \partial|\hat{s}'|/\partial x$ (symbols refer to theoretical results) together with DNS results for case B^{11} from figure 9(*b*) (lines).

place at the wall in the DNS or close to it as with the roughness elements (spacers) in the experiment and therefore remains slightly suboptimal. Thus, the present DNS data confirm for an FPG boundary layer what has been found experimentally by (Fransson *et al.* 2004, cf. § IV.C) for a ZPG boundary layer.

Case B_{02} is the optimal DNS case in the sense that it requires the lowest forcing amplitude (table 1) to reach the same amplitude as all other cases. Even though this case possesses the same $\hat{u}'$-amplitude functions as the other cases (as pointed out in § 4.1), it bears no resemblance with optimally growing theoretical results in the FPG region. Three brief conclusions can be drawn from this. First, if we want a large $\hat{u}'$ from wall forcing but not necessarily its downstream growth, it is advantageous to locally trigger the lift-up effect as in case B_{02}. Second, if we want to continuously trigger the lift-up effect and transient growth using near-wall forcing, exciting a pair of oblique waves as in case B^{11} is most efficient. Third, if we want overall optimal growth, we have to apply disturbance forcing away from the wall.

5.1.3. *Modal instability*

For a discussion of the region of modal instability we focus first on the $x_0 = -0.45$ case only. As before, we apply (4.1) to obtain the disturbance-velocity components $\hat{u}'_{\parallel}$, $\hat{v}'_{\perp}$. Amplitudes and growth rates of these two components as well as $|\hat{w}'|_{outer}$ are given in figure 13.

At separation S, the close(st) matching of amplification rate (figure 13*b*) and amplitude functions (figure 14, upper panels) between the boundary-layer calculation and the DNS/experiment can be observed. Agreement inside the LSB (figure 14) is roughly independent on the inflow position x_0 of the optimal disturbance.

5.1.4. *Validity of the linearized boundary-layer equations inside the LSB*

Deeper inside the LSB ($x > 0.3$), DNS results indicate a stronger importance of transient growth and eventually exhibit a vanishing modal growth of the steady three-dimensional disturbance. Results from the linearized boundary-layer equations fail to exhibit vanishing modal growth. Nevertheless, $|\hat{u}'|_{max}$ and (inner, i.e. overall) $|\hat{v}'|_{max}$ (figure 11*b*) as well as amplitude functions (figure 14) remain reasonably close even at $x = 0.33$.

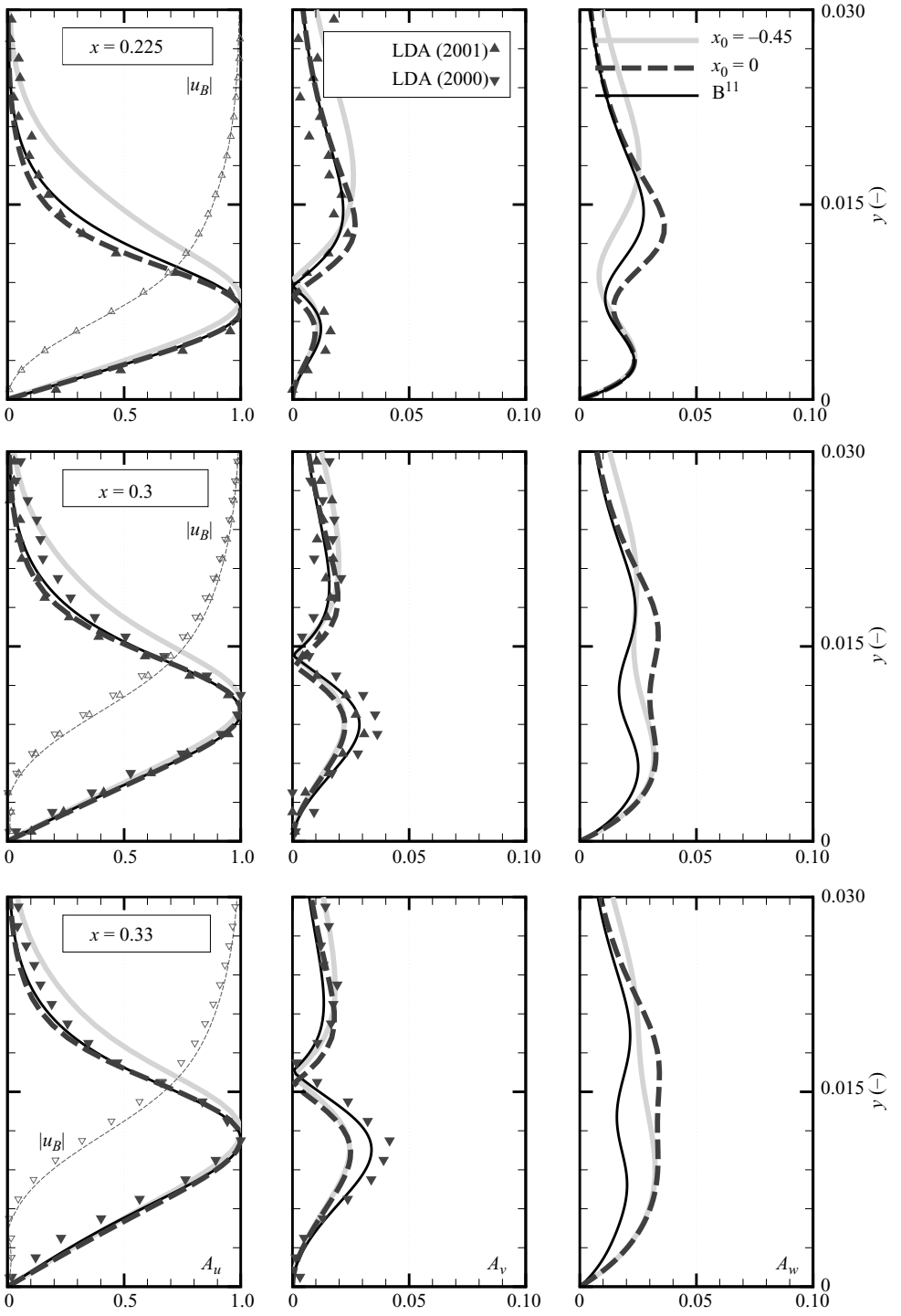

FIGURE 14. Velocity amplitudes of mode (0, 2), normalized by the respective $|\hat{u}'|_{max}$. Comparison of results for $x = 0.225, 0.3, 0.33$ from DNS (B^{11}, thin black lines) and optimal perturbations ($x_0 = -0.45$, grey lines; $x_0 = 0$, dashed lines) with measurements (symbols).

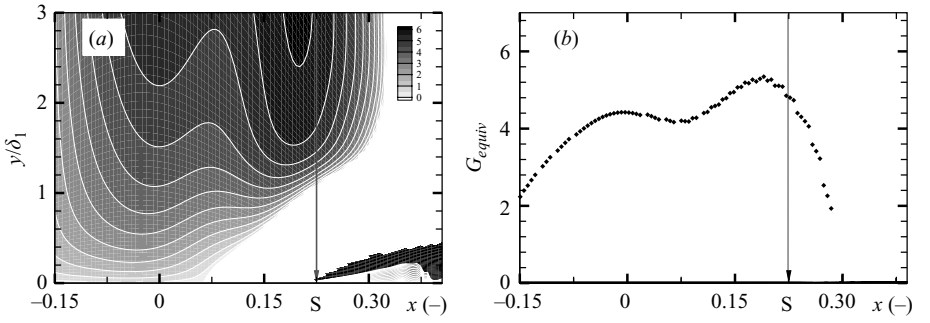

FIGURE 15. Quantities computed from the DNS base flow. (*a*) Contours of equivalent Görtler number G_{equiv}. (*b*) Equivalent Görtler number G_{equiv} along x at constant $y/\delta_1 \approx 1.4$.

No convergence could be obtained when the outflow location x_1 was moved further downstream than $x_1 = 0.3348$. All present observations suggest that the boundary-layer computations are valid at the separation location but not too far beyond it.

5.2. *Instability mechanism at the onset of modal growth: Görtler-type instability*

The parabolic boundary-layer equations solved earlier (§ 5.1) can handle transient growth associated with a superposition of several (mostly or exclusively damped) eigenmodes on the one hand and modal growth associated with a single amplified eigenmode on the other. We now want to seek evidence for the hypothesis that the existence of a single amplified eigenmode is due to a Görtler-type instability.

As discussed in the introduction (§ 1.1.1), occurrence of concave streamline curvature in a boundary-layer flow is a key requirement for a Görtler-type instability. Streamline curvature is connected to $\partial_x V$. To evaluate the role of streamline curvature upstream and around S, the curvature is quantified from the mean flow by means of an equivalent Görtler number G_{equiv}. As in more recent approaches in Görtler theory (Lee & Liu 1992; Cossu *et al.* 2000) we can imagine including a wall-curvature term in the linearized boundary-layer equations that contains the Görtler number G. Hence, with a non-zero G, these equations would contain a term of the form (base flow $\boldsymbol{v}_B{}^T = [U\ V]^T = [u_B\ v_B]^T$)

$$\gamma^2(2G^2U + \partial_x V) \times \hat{u}'.$$

This implies the following definition of an equivalent Görtler number $G_{eq} = G_{eq}(x, y)$:

$$2G_{eq}^2 U \doteq (2G^2U + \partial_x V). \tag{5.1}$$

For flow over a curved wall with negligible streamwise evolution ($\partial_x V \ll 2G^2U$) we have $G_{eq} = G$. For sufficiently strong streamline curvature along a straight wall ($\partial_x V \gg 2G^2U$) we have $G_{eq} = \sqrt{\partial_x V/(2U)}$ instead. To allow for $\partial_x V < 0$, a refined definition of the equivalent Görtler number ($G = 0$) will be used in the following:

$$G_{equiv}(x, y) \doteq \mathrm{sign}(\partial_x V)\sqrt{|\partial_x V|/2U}. \tag{5.2}$$

With this definition, (only) positive G_{equiv} corresponds to a concave curvature.

From $x = -0.15$ onwards, G_{equiv} is seen to increase along x up to $x = 0$ (figure 15*a*). It reaches a plateau, or more precisely a local minimum, around $x = 0.075$ until it climbs to an overall maximum only slightly upstream of S. Downstream of S, it quickly drops again. If we follow G_{equiv} at a distance $y/\delta_1 \approx 1.4$ (figure 15*b*) we see a

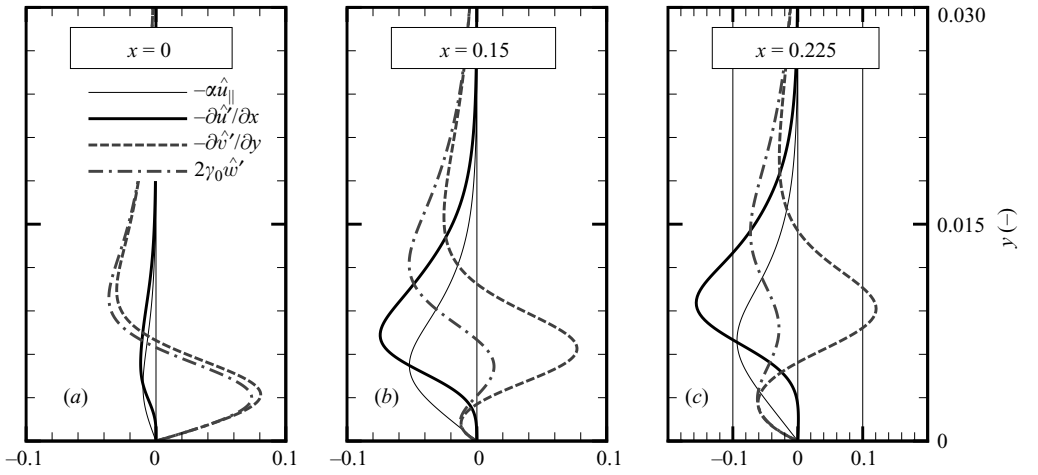

FIGURE 16. Terms of the continuity equation (thick lines) and $-\alpha\hat{u}'_{\parallel}$ (thin line) for mode (0, 2) at (*a*) $x = 0.0$, (*b*) $x = 0.15$ and (*c*) $x = 0.225$.

resemblance to the curve with amplification rates α from $|\hat{v}'_{\perp}|_{max}$ or $|\hat{w}'|_{outer}$ of DNS (see e.g. figure 9*b*).

The Görtler-type instability can only be expected in the part of the flow further away from the wall, since it is only there that G_{equiv} possesses appreciable values (figure 15*a*), in particular around S. This is consistent with a sketch in Inger (1987) (1987; cf. figure 5). This observation also suggests to indeed consider $|\hat{w}'|_{outer}$ rather than $|\hat{w}'|_{inner}$ to compute growth rates of the Görtler instability.

5.3. *Disturbance-shape evolution in the strongly non-parallel flow*

The peak in values of the equivalent Görtler number (figure 15) in conjunction with the collapse of transformed amplification rates from DNS and theory (figure 13) suggests the onset of modal growth to be located slightly upsteam of $x = 0$. At this onset, the disturbance takes the familiar form of a 'local' streamwise vortex as known from Görtler instability in attached, self-similar boundary layers (compare e.g. our respective amplitude functions with figure 2 in Lee & Liu 1992). However, slightly upstream of S and inside the LSB we do not see the shape of a 'local' vortex anymore (figure 14), and this motivates a closer inspection.

5.3.1. *The streak component*

Downstream of $x = 0$, the strong APG causes the mean flow to turn away from the wall. The streamwise vortex and its accompanying $\hat{u}'$-streak turn in a similar way (figure 18). Since the streak (or more precisely its wall-normal maximum) moves away from the wall, its growth ($= \partial|\hat{u}'|/\partial x$) must be stronger further away from the wall. This is exactly what we see in figure 16(*b*, *c*) if we compare $\alpha\hat{u}'_{\parallel}$ and $\partial\hat{u}'/\partial x$. Vanishing growth in $|\hat{u}'|$ close to the wall can be understood based on the lift-up effect together with the fact that v' changes its sign along y (figure 17).

5.3.2. *The vortex components*

At $x = 0$, the mean flow is essentially wall-parallel, and the streamwise growth of the disturbance is small. Hence, $\hat{u}'$ does not notably contribute to the continuity equation and $\partial\hat{w}'/\partial z = 2\gamma_0\hat{w}'$ agrees well with $-\partial\hat{v}'/\partial y$ (figure 16*a*). In a visualization,

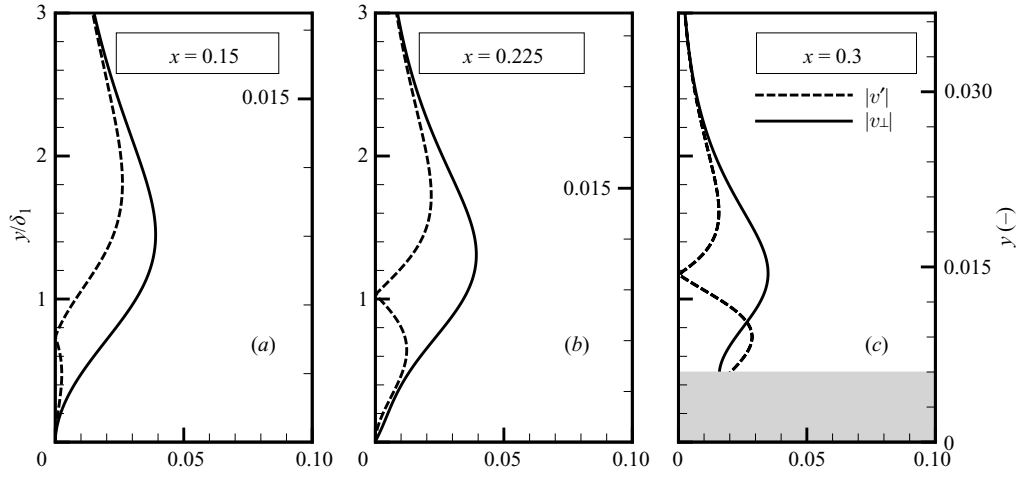

FIGURE 17. Velocity amplitudes $|\hat{v}'|$ (dashed line) and $|\hat{v}'_{\perp}|$ (solid line) of mode (0, 2), normalized by $|\hat{u}'|_{max}$ and $|\hat{u}'_{\parallel}|_{max}$, respectively; DNS for case B^{11} for (*a*) $x = 0.15$, (*b*) $x = 0.225$, (*c*) $x = 0.3$. The region below the dividing streamline is blanked in (*c*) (grey box).

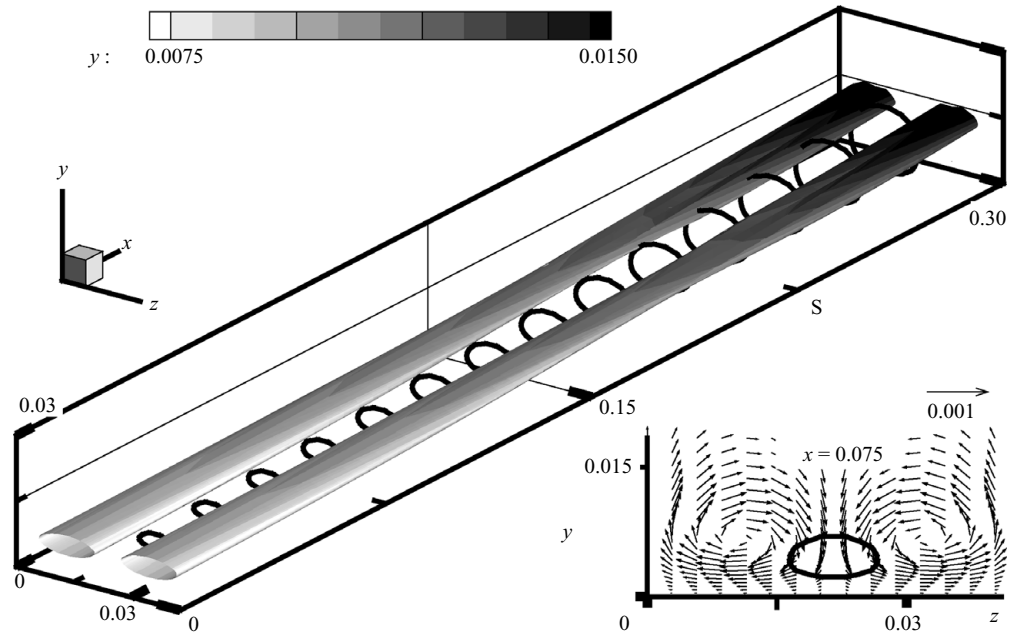

FIGURE 18. Vortex visualization using isosurfaces of $\lambda_2 = -0.0085$ (for a definition of λ_2 see Jeong & Hussain 1995), computed from the disturbance flow only, case B_{11}. The isosurface is coloured by the distance from the wall (greyscale) and shown together with isolines $\hat{u}' = 0.01$ in planes $x = \text{const.}$ (black rings). The insert (lower right corner) depicts in-plane velocity vectors at $x = 0.075$.

we see the corresponding streamwise vortex with its axis parallel to the wall at $x = 0$ (figure 18).

At $x = 0.15$, the streamwise vortex already points away from the wall. Growth and absolute amplitude of $\hat{u}'$ are now sufficiently strong so that $2\gamma_0\hat{w}'$ and $-\partial\hat{v}'/\partial y$ differ except very close to the wall and in the free stream (figure 16*b*). If we consider

transformed variables instead and normalize the wall-normal coordinate y by the displacement thickness δ_1, we see that $\hat{v}'_\perp$ keeps the same shape until into the LSB, with its maximum around $y/\delta_1 \approx 1.4$ (compare *a*, *b* and *c* in figure 17). This shape closely resembles the one at $x = 0$ (figure 17*a* versus the lower centre panel of figure 6), where $\hat{v}'_\perp \approx \hat{v}'$. The fact that $\hat{v}'_\perp$ (and similarly also $\hat{u}'_\parallel$) keeps its shape is another argument in favour of a Görtler-type mechanism active beyond $x = 0$, in addition to the growth-rate-based argument of § 5.2.

Due to the fact that the $\hat{u}'_\parallel$-streak occurs at an angle to the wall, it transports fluid to and away from the wall. Together with its strong growth, this causes a local streamwise vortex very close to the wall at certain x-positions (e.g. observe the shape of $\hat{u}'$, $\hat{w}'$ in figure 16*b* and $\hat{v}'$ in figure 17*a*). This vortex is located underneath the main Görtler vortex and rotates in the opposite direction. As a result, the main vortex gets slightly distorted at, and downstream of, S (figure 18). The connection between $\hat{v}'$ and $\hat{w}'$ close to the wall can be seen quite well in figure 16(*b*, *c*) for $y < 0.003$. It explains why we observed $\hat{v}'_{inner}$ and $\hat{w}'_{inner}$ growing together around S in § 4.2. This explanation also justifies to discard $\hat{w}'_{inner}$ when computing growth rates of the Görtler instability as was done in § 4.2.

5.3.3. *Downstream of the modal-instability region*

Even though the instability eventually vanishes, the upper (decaying) vortex still causes a growing $\hat{u}'_\parallel$ due to the lift-up effect. In turn, this $\hat{u}'_\parallel$ results in a growing $|\hat{u}'|$ and $|\hat{v}'|$. Near the wall, shapes of the streamwise and wall-normal velocity components are indeed remarkably similar (figure 19), both being a result of $\hat{u}'_\parallel$.

6. Summary and conclusions

The streamwise evolution of steady linear three-dimensional spanwise-harmonic disturbances has been investigated in a laminar boundary layer with a favourable-to-adverse pressure gradient. The flow eventually undergoes separation. Three different investigation methods are applied: an experiment, DNSs and a method based on optimal disturbances of the linearized boundary-layer equations.

All three methods exhibit a close agreement with respect to disturbance shape and evolution for the entire streamwise domain. The linearized boundary-layer equations turned out to be applicable even at separation, failing only deep inside the bubble.

Two different fundamental mechanisms can explain the streamwise disturbance evolution: spatial transient growth and a modal Görtler-type instability. In certain parts of the domain both effects are blended and contribute simultaneously to the disturbance shape. In both mechanisms, the lift-up effect feeds growth of the streamwise velocity component.

Non-modal disturbance evolution is observed in the stable FPG region. Corresponding physical processes are analogous to those known to occur in ZPG boundary layers. Transient growth is not observed in the DNS in case of steady wall blowing and suction. Nevertheless even then a strong streak results near the wall due to local lift-up.

Around the start of the APG region a modal instability sets in. It can be distinguished from transient growth by decomposing the disturbance vector into components parallel and normal to the base flow instead of parallel and normal to the wall. With such a decomposition, all three resulting components are seen to grow alike further away from the wall, for cases in which transient effects do not contribute to the disturbance evolution.

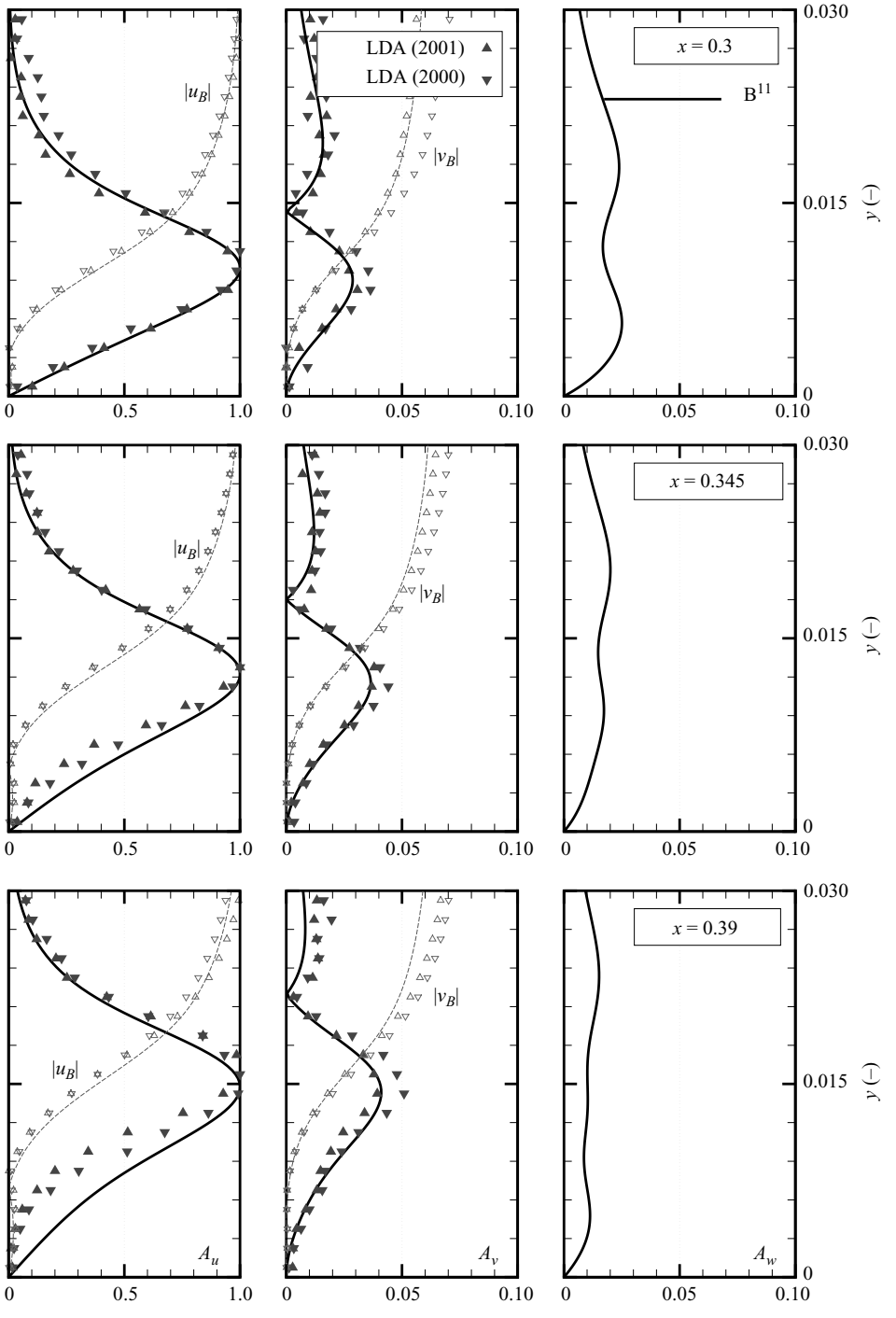

FIGURE 19. Same as figure 6. Comparison of results for case B^{11} with measurements inside the LSB for $x = 0.3, 0.345, 0.39$. Base-flow quantities u_B, v_B are also shown.

The onset of instability is due to streamline curvature; i.e. it is of Görtler type. Based on a qualitatively good correlation of the growth rate and an equivalent Görtler number as well as on the shape of the amplitude functions, streamline curvature remains the most probable dominating source of instability even at separation and inside the bubble. Therefore, we have not only presented strong evidence that a Görtler instability can be active in a separation bubble but have also reported, for the first time, respective growth rates.

Once streamline curvature and modal instability vanish deeper inside the bubble, we observe transient growth caused by the lift-up effect again. Hence, we have shown that spatial modal growth (of Görtler type) of steady disturbances can be followed by notable spatial transient growth. Disturbance growth is therefore sustained downstream of the neutral stability curve. Together with evidence that transient growth is important also at the onset of the instability, this suggests that the neutral point may be irrelevant for a Görtler-type instability. Unlike in the FPG region, this transient growth occurs in the streamwise and the wall-normal disturbance velocity component as the mean flow points away from the wall.

Non-parallel effects are observed in the APG region and at separation, influencing the amplitude functions in particular close to the wall. This underlines that observations about streamwise vortices made in attached parallel flows are not necessarily transferable to separating flows in a straightforward or simple way. The amplitude functions of the streamwise velocity in the region of FPG were found to be largely independent of the mechanism of disturbance excitation in DNS and experiment. Differences in amplitude functions of the wall-normal velocity, on the other hand, were found to be significant. Amplitude functions of the streamwise velocity alone are insufficient to explain the dynamics of the flow.

OM would like to thank Markus Kloker, Universität Stuttgart and Xuesong Wu, Imperial College London, for useful discussions and Johan Larsson, Stanford University, for useful comments on the manuscript. Financial support of this research by the Deutsche Forschungsgemeinschaft (German research foundation) under grant Ri 680/10-1 and Ma 3916/1-1 and by the Deutscher Akademischer Austauschdienst (DAAD) under grant PPP Schweden is gratefully acknowledged.

REFERENCES

Andersson, P., Berggren, M. & Henningson, D. S. 1999 Optimal disturbances and bypass transition in boundary layers. *Phys. Fluids* **11** (1), 134–150.

Boiko, A. V. 2002 Development of a stationary streak in a local separation bubble. *Tech Rep.* IB 224–2002 A04. German Aerospace Center (DLR), Institute for Fluid Mechanics.

Bottaro, A. & Luchini, P. 1999 Görtler vortices: are they amenable to local eigenvalue analysis? *Eur. J. Mech.* B **18** (1), 47–65.

Cossu, C., Chomaz, J.-M., Huerre, P. & Costa, M. 2000 Maximum spatial growth of Görtler vortices. *Flow Turbul. Combust.* **65**, 369–392.

Ellingsen, T. & Palm, E. 1975 Stability of linear flow. *Phys. Fluids* **18** (4), 487–488.

Floryan, J. M. & Saric, W. S. 1982 Stability of Görtler vortices in boundary layers. *AIAA. J.* **20** (3), 316–324.

Fransson, J. H. M., Brandt, L., Talamelli, A. & Cossu, C. 2004 Experimental and theoretical investigation of the nonmodal growth of steady streaks in a flat plate boundary layer. *Phys. Fluids* **16** (10), 3627–3638.

Görtler, H. 1941 Instabilität laminarer Grenzschichten an konkaven Wänden gegenüber gewissen dreidimensionalen Störungen. *ZAMM* **21** (4), 250–252.

Inger, G. R. 1987 Spanwise-periodic three-dimensional disturbances in the wake of a slightly stalled wing. *Paper* 87-0456. AIAA.

Jeong, J. & Hussain, F. 1995 On the identification of a vortex. *J. Fluid Mech.* **285**, 69–94.

Kachanov, Y. S. & Levchenko, V. Y. 1984 The resonant interaction of disturbances at laminar-turbulent transition in a boundary layer. *J. Fluid Mech.* **138**, 209–247.

Klebanoff, P. S., Tidstrom, K. D. & Sargent, L. M. 1962 The three-dimensional nature of boundary-layer instability. *J. Fluid Mech.* **12**, 1–34.

Kloker, M. 1998 A robust high-resolution split-type compact FD scheme for spatial direct numerical simulation of boundary-layer transition. *Appl. Sci. Res.* **59**, 353–377.

Landahl, M. T. 1975 Wave breakdown and turbulence. *SIAM J. Appl. Math* **28** (4), 735–756.

Landahl, M. T. 1980 A note on an algebraic instability of inviscid parallel shear flows. *J. Fluid Mech.* **98**, 243–251.

Lang, M. 2005 Experimentelle Untersuchungen zur Transition in einer laminaren Ablöseblase mit Hilfe der Laser-Doppler-Anemometrie und der Particle Image Velocimetry. Dissertation, Universität Stuttgart, Stuttgart, Germany.

Lang, M., Rist, U. & Wagner, S. 2004 Investigations on controlled transition development in a laminar separation bubble by means of LDA and PIV. *Exp. Fluids* **36**, 43–52.

Lee, K. & Liu, J. T. C. 1992 On the growth of mushroomlike structures in nonlinear spatially developing Goertler vortex flows. *Phys. Fluids* A **4** (1), 95–103.

Levin, O., Chernoray, V. G., Löfdahl, L. & Henningson, D. S. 2005 A study of the Blasius wall jet. *J. Fluid Mech.* **539**, 313–347.

Levin, O. & Henningson, D. S. 2003 Exponential vs algebraic growth and transition prediction in boundary layer flow. *Flow Turbul. Combust.* **70**, 183–210.

Luchini, P. 2000 Reynolds-number-independent instability of the boundary layer over a flat surface: optimal perturbations. *J. Fluid Mech.* **404**, 289–309.

Luchini, P. & Bottaro, A. 1998 Görtler vortices: a backward-in-time approach to the receptivity problem. *J. Fluid Mech.* **363**, 1–23.

Marxen, O. 2005 Numerical studies of physical effects related to the controlled transition process in laminar separation bubbles. Dissertation, Universität Stuttgart, Stuttgart, Germany.

Marxen, O., Rist, U. & Henningson, D. 2006 Steady three-dimensional streaks and their optimal growth in a laminar separation bubble. In *New Results in Numerical and Experimental Fluid Mechanics V* (ed. H. J. Rath, C. Holze, H.-J. Heinemann, R. Henke & H. Hönlinger), Notes on Numerical Fluid Mechanics and Multidisciplinary Design (NNFM), vol. 92, pp. 233–240. Springer.

Marxen, O., Rist, U. & Wagner, S. 2004 Effect of spanwise-modulated disturbances on transition in a separated boundary layer. *AIAA J.* **42** (5), 937–944.

Pauley, L. L. 1994 Response of two-dimensional separation to three-dimensional disturbances. *J. Fluids Engng* **116**, 433–438.

Rist, U. 1998 Zur Instabilität und Transition in laminaren Ablöseblasen. Habilitation, Universität Stuttgart, Stuttgart, Germany.

Rist, U. 2002 On instabilities and transition in laminar separation bubbles. In *Proceedings of the CEAS Aerospace Aerodynamics Research Conference*, Cambridge, UK.

Rist, U. 2003 Instability and transition mechanisms in laminar separation bubbles. In *VKI/RTO-LS 'Low Reynolds Number Aerodynamics on Aircraft Including Applications in Emerging UAV Technology'*, pp. 1–29. Van Kármán Institut.

Rist, U. & Augustin, K. 2006 Control of laminar separation bubbles using instability waves. *AIAA J.* **44** (10), 2217–2223.

Saric, W. S. 1994 Görtler vortices. *Annu. Rev. Fluid Mech.* **26**, 379–409.

Schmid, P. J. & Henningson, D. S. 2001 *Stability and Transition in Shear Flows*, 1st edn. Springer.

Spalart, P. R. & Strelets, M. K. 2000 Mechanisms of transition and heat transfer in a separation bubble. *J. Fluid Mech.* **403**, 329–349.

Trefethen, L. N., Trefethen, A. E., Reddy, S. C. & Driscoll, T. A. 1993 Hydrodynamic stability without eigenvalues. *Science* **261**, 578–584.

Watmuff, J. H. 1999 Evolution of a wave packet into vortex loops in a laminar separation bubble. *J. Fluid Mech.* **397**, 119–169.

Wilson, P. G. & Pauley, L. L. 1998 Two- and three-dimensional large-eddy simulations of a transitional separation bubble. *Phys. Fluids* **10** (11), 2932–2940.